Biomaterials 201 (2019) 33–41

Contents lists available at ScienceDirect

Biomaterials

journal homepage: www.elsevier.com/locate/biomaterials

Assembly of upconversion nanophotosensitizer *in vivo* to achieve scatheless real-time imaging and selective photodynamic therapy

Yansong Feng[a], Yanni Wu[a], Jing Zuo[a], Langping Tu[b], Ivo Que[c], Yulei Chang[b,**], Luis J. Cruz[c], Alan Chan[c], Hong Zhang[a,*]

[a] *Van 't Hoff Institute for Molecular Sciences. University of Amsterdam, Science Park 904, 1098 XH, Amsterdam, the Netherlands*
[b] *State Key Laboratory of Luminescence and Applications. Changchun Institute of Optics Fine Mechanics and Physics, Chinese Academy of Sciences. Changchun, 130033, Jilin, China*
[c] *Translational Nanobiomaterials and Imaging, Department of Radiology, Leiden University Medical Center, 2333, Percuros B.V, Leiden, the Netherlands*

ARTICLE INFO

Keywords:
Bioorthogonal chemistry
Upconversion luminescence
Real-time imaging
Switchable photodynamic therapy

ABSTRACT

A perfect "off" to "on" switch of the therapeutic function is very important to minimize the phototoxicity of nanoplatforms assisted imaging-guided photodynamic therapy (PDT) of cancer. Current approaches rely on preloaded photosensitizers, where the off/on state of PDT is regulated by the sensitizing light of photosensitizers. However, the photoactivities inevitably occur when imaging/diagnosis or exposure to sunlight, *etc*. These preloading approaches will cause the damage to normal cells and the photosensitivity to the skin. Taking upconversion photodynamic therapy as an example we report here a biorthogonal chemistry solution to circumvent this problem. The luminescence upconversion nanoparticles (UCNPs) are anchored with one handle of click reaction and targeting entity, these nanoplatforms enable the imaging/labelling/tracking, especially for imaging-guided surgery. Once they are targeted, the photosensitizers armed with the other match handle will be injected *in situ* and click reaction will occur between the two handles to link the photosensitizers closely with the targeted nanoplatforms in a very short time, enabling the PDT function of the nanoplatforms. Proof of principle has been demonstrated *in vitro* and *in vivo*. This approach can be readily extended to chemotherapy, radiotherapy, *etc.* to overcome the side effect of these therapies of cancers.

1. Introduction

Photodynamic therapy (PDT) is one of the main modalities of cancer treatment in clinic [1–3]. Compared with other modalities this light-induced therapy is minimally invasive and the treatment can be well controlled in location and time [4,5]. With the advance of nanotechnology, PDT with the aid of nanoparticles is intensively exploited [6,7]. Sensitizer uploaded nanoparticles can be mounted with targeting vectors, *e.g.* antibodies, enabling imaging-guided PDT with high specificity [8–10]. However, till now PDT is in clinic limited to the superficial cancers due to the necessity of UV or visible light in generating reactive oxygen species (ROS) [11]. In addition, in some complex biological systems such as skin, brain, soft tissues, fibrous tissues and fatty tissues, light of such short wavelength may bring the concern on the interference of biological self-fluorescence, light scattering and tissue damage [12,13]. Near-infrared (NIR) light transduction was thus introduced in to circumvent this problem, *e.g.* employing the property of NIR light excitation of lanthanide-doped upconversion nanoparticles (UCNPs) [14].

UCNPs make NIR light possible to induce PDT, which significantly extends the PDT to deep-seated tumors [14–17]. Popular approach is to covalently anchor the photosensitizers to the UCNPs forming theranostic nanoplatforms, wherein imaging and therapeutic functions are integrated in one nanoplatform, so-called "all-in-one" strategy [15,16,18]. There are, however, cases in which the imaging and therapy functions need to be separated. For example, during surgery of cancer, the surgeon requires only the indication of the margin of cancer and in this case imaging of the UCNPs is sufficient, whereas PDT is not necessary. PDT can be used as post-operational therapy to prevent the recurrence of cancer [19–21]. Besides, the "all-in-one" strategy has the drawback that during the targeting process phototoxicity of normal cells might be induced by light, leakage of the photosensitizers, *etc.* Therefore, to realize a switch between "off" and "on" is important and interesting for cancer administration [22,23].

* Corresponding author.
** Corresponding author.
E-mail addresses: yuleichang@ciomp.ac.cn (Y. Chang), h.zhang@uva.nl (H. Zhang).

https://doi.org/10.1016/j.biomaterials.2019.02.015
Received 9 November 2018; Received in revised form 25 January 2019; Accepted 12 February 2019
Available online 13 February 2019
0142-9612/

Up to now, UCNPs based approaches in realizing PDT switch are limited, *e.g.* change of the excitation wavelength, employing luminescence quencher to quench the upconversion emission during the targeting process, or self-assembling the UCNPs and photosensitizers together, subsequently disassembling into individual UCNPs and free photosensitizers upon stimuli-responsive [24,25]. All these approaches are, however, unable to realize photosensitizer-free when the PDT is "off", thus the above-mentioned concern on "all-in-one" strategy remains.

Bioorthogonal chemical reaction offers here a new possibility in realizing the switch between real-time imaging and PDT. Bioorthogonal chemical reaction is a sort of chemical reactions in bio-system with high yields with limited by-products, which has no effect on native biological processes [26–29]. Owing to the merits of high selectivity, high speed and ease [30,31], it is ideal for biomolecules such as the radiolabeling of molecules, the site-specific bio-conjugation and *in vivo* pretargeting strategies in living systems without cellular toxicity [32,33]. Given by these, the inverse-electron-demand Diels-Alder cycloadditions involving tetrazine (Tz) and strained alkenes is one example, which usually does not need catalyst because of the fast enough kinetics. Regarding the strained alkenes, the commercial norbornene (NB, with an amino group) is a good candidate for further conjugation with organic dyes and photosensitizers.

In this work, we introduce a bioorthogonal chemistry solution to realize PDT "off" and "on" switching. We take luminescence UCNPs as the optical imaging agent and the internal energy transducer, and later to bind photosensitizers on their surface to construct the nanophotosensitizers *via* a bioorthogonal chemical reaction. The nanophotosensitizers formed *in vivo* can be triggered by the NIR light to perform an effective PDT. The principle of our approach is illustrated in Scheme 1, where UCNPs are covalently bonded with pretargeting molecule and one handle of the bioorthogonal reaction Tz, to form UCNPs-Tz/FA-PEG. The UCNPs-Tz/FA-PEG can be specifically targeted to the cancer cells. Under NIR light irradiation, these nanoplatforms shall perform as a contrast agent for imaging only. Once the other handle of the bioorthogonal reaction, NB, which is conjugated with photosensitizer rose bengal, *i.e.* RB-NB, is injected, the photosensitizing RB-NB will be combined to the imaging nanoplatform (UCNPs-Tz/FA-PEG) due to the efficient click reaction between the Tz and NB. Effective energy transfer (ET) between UCNP and the RB enables a PDT with high efficacy. *In vitro* and *in vivo* tests have validated the proof of principle of this approach. This approach can be readily extended to nanomaterials assisted chemotherapy, radiotherapy or other therapies.

2. Experimental section

2.1. Reagents

$RECl_3{\cdot}6H_2O$ (Er, Yb, Y > 99%), oleic acid (OA), oleylamine (OM), 1-octadecene (ODE), $(CF_3COO)_3Y$, CF_3COONa, NaOH, NH_4F, poly(allylamine) (PAAm), $Zn(OTf)_2$, 4-Cyanophenylacetic acid, anhydrous hydrazine, sodium nitrite, folic acid, *N*-hydroxy-succinimide, 1-ethyl-3-(3-dimethylaminopropyl) carbodiimide, PEG-SC, norbornylene (NB), fluorescein isothiocyanate (FITC), methanol, ethanol, acetone, cyclohexane, *N*,*N*-Dimethylformamide (DMF), dimethyl sulfoxide (DMSO), ethyl acetate and sodium sulfate were purchased from Sigma-Aldrich. All the chemicals were used without further purification. The MCF-7 cell lines were acquired from Leiden University Medical Center.

2.2. Surface functionalization of UCNPs

The hydrophilic NH_2-functionalized UCNPs were obtained *via* a ligand exchange to phase transfer. Firstly, 4 mL as-synthesized UCNPs dispersed in cyclohexane and 4 mL 0.1 M HCl was reacted for 4 h, after washed with water for two times, 200 μL PAAm (20 wt%) aqueous solution was added in 4 mL DMF. Then the mixture was reacted with stirring for 24 h. The nanoparticles were washed with water and DMF. Finally, the amino-functionalized UCNPs were obtained and dispersed in DMF.

2.3. Covalent conjugation of UCNPs with tetrazine and folic acid

4,4'-(1,2,4,5-tetrazine-3,6-diyl) dibenzoic acid was synthesized according to literature methods [34]. 0.25 mmol $Zn(OTf)_2$, 0.26 mL (5.0 mmol) of 4-Cyanophenylacetic acid, and 0.8 mL (25.0 mmol) of anhydrous hydrazine were added in 10 mL microwave reaction tube. After reaction at 60 °C for 24 h the solution was cooled down to 25 °C. 5 mL water with sodium nitrite (10 mmol, 690 mg) was added by dropwise, followed by 1 M HCl added carefully. Addition of 1 M HCl continued until gas evolution ceased and the pH value is 3. The mixture was extracted with ethyl acetate and dried with sodium sulfate. The ethyl acetate was evaporated using rotary evaporation and purified

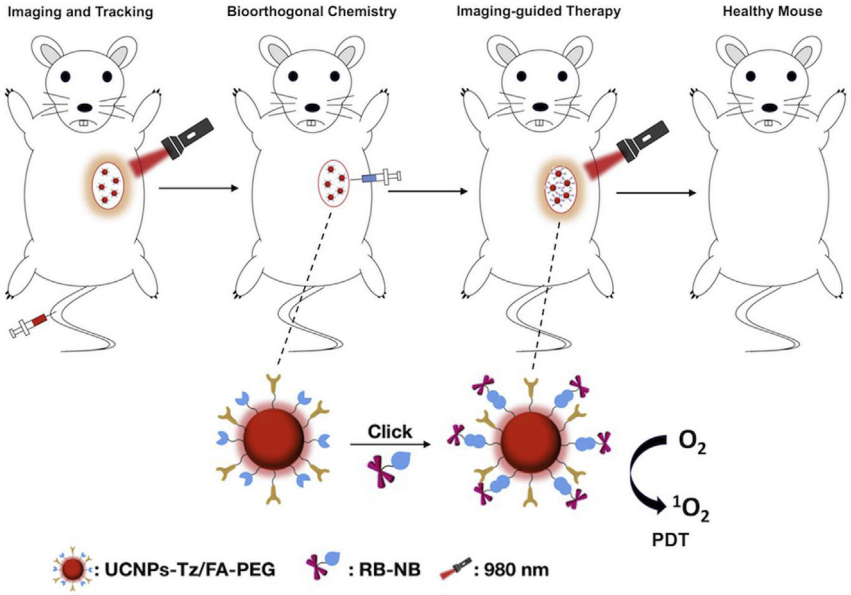

Scheme 1. Schematic illustration of UCL imaging/tracking and selective PDT by bioorthogonal chemistry.

using silica column chromatography. ^{1}H NMR (300 MHz, $CDCl_3$) δ 7.66 (d, J = 8.3 Hz, 4H), 7.43 (d, J = 8.2 Hz, 4H). calc. for $C_{16}H_{10}N_4O_4$: MS m/z: 321.1 [M+] (calcd: 322.1). The synthesis route was shown in Fig. S1.

To modify tetrazine covalently to amino-functionalized $NaYF_4$: 2% Er, 20% Yb @ $NaYF_4$, 0.8 mg tetrazine, 0.5 mg folic acid, 1 mg *N*-hydroxy-succinimide and 1 mg 1-ethyl-3-(3-dimethylaminopropyl) carbodiimide were incubated in 5 mL DMF at 25 °C for 2 h. Followed 10 mg of amino-functionalized UCNPs was added and reacted for 24 h. After that, UCNPs-Tz/FA was obtained and then washed with DMF to remove the unreacted tetrazine. Finally, 10 mg PEG-SC and 10 mg UCNPs-Tz/FA were reacted in 15 mL DMSO and 5 mL ethanol for 24 h. After washed with water twice the nanoparticles finally were dispersed in PBS to get the nanoplatform UCNPs-Tz/FA-PEG. The nanoplatforms without tetrazine (UCNPs-FA-PEG) are synthesized in the same method.

2.4. Click reaction in different solvents

Tetrazine was mixed with a specific activity norbornylene in different solvents (DMSO, methanol, and PBS) in the cuvette and detected the UV–vis spectrum of the tetrazine at selected times. The cycloaddition yields and reaction rate were determined from absorption intensity change of the tetrazine.

2.5. Click reaction on the surface of the nanoparticles

5 mL of 2 mg/mL UCNPs-Tz/FA-PEG reacted with different amount of RB-NB (1%, 2%, 3% and 10% w/w) for 15 min to form UCNPs-C-RB conjugates, for comparison, we also made the nanoparticles UCNPs-FA-PEG mixed with different amount of RB-NB by electrostatic interaction. The nanoconjugates washed with DMF twice and water in order to remove the unreacted RB-NB, followed by centrifugal separation. The loading capacity of photosensitizers of each UCNP was calculated according to the absorption intensity of RB.

2.6. Singlet oxygen detection ($^1O_2$)

$^1O_2$ was determined by DPBF followed as reported protocol. 2 mL of as-obtained UCNPs-Tz/FA-PEG-RB or UCNPs-FA-PEG&RB (2 mg/mL) dissolved in water and 10 μL (1 mg/mL) of DPBF-ethanol solution were added which was kept in dark overnight. The absorption intensity of DPBF at 410 nm was recorded every 3 min after irradiated by 980 nm lasers light (3, 6, 9, 12, 15 and 18 min) at the same power density (0.7 W/cm^2).

2.7. Click reaction and PDT in vitro

Breast carcinoma MCF-7 cells were maintained in the DMEM under 5% CO_2 atmosphere at 37 °C. The cells were firstly incubated in the 96-well plate (1×10^4 per well) for 24 h. After that, UCNPs-Tz/FA-PEG or UCNPs-FA-PEG was added in the cells with different concentrations (0, 50, 100, 200, 400 μg/mL), each with five parallel. The cell viability was investigated using a standard MTS assay.

For the click reaction experiment *in vitro*, the cells were incubated in the special plates which could be used for confocal microscopy. Then cells were incubated with 100 μg/mL UCNPs-Tz/FA-PEG or UCNPs-FA-PEG for 4 h at 37 °C. After three times washing with PBS, 5 μg FITC-NB was added to achieve the click reaction at the determined time (0 min, 10 min, and 20 min). Finally, the cells were stained with DAPI and rinsed with PBS three times and monitored by confocal microscopy.

For the PDT studies, the cells were firstly incubated in the 96-well plates with UCNPs-Tz/FA-PEG or UCNPs-FA-PEG (50, 100, 150 or 200 μg/mL) for 4 h and followed washed by PBS, then reacted with RB-NB. The saline, UCNPs-Tz/FA-PEG or UCNPs-FA-PEG, and only with the laser group were incubated for 48 h as the control experiments. A CW 980 nm laser was used to irradiate the cells for 15 min at a density of 0.7 W/cm^2. After that, the cells were cultured for another 48 h. After various treatment, the click reaction mediated PDT efficacy was evaluated by MTS assay.

2.8. Flow cytometry

In the flow cytometry analysis, the cells were trypsinized and stained by Annexin V-FITC and propidium iodide (Annexin V-FITC Apoptosis Staining/Detection Kit) in order to detect the cell apoptosis.

Annexin-V-fluorescein isothiocyanate (FITC) and propidium iodide (PI) staining were performed using an Annexin-V-FITC/PI kit (BD) according to the manufacturer's instructions. Briefly, MCF-7 cells were cultured in 6-well plates and then treated with different reagents (PBS or UCNPs-FA-PEG or UCNPs-Tz/FA-PEG or “Always On”) for 4 h, each with 3 parallel, then the cells in group UCNPs-Tz/FA-PEG or UCNPs-FA-PEG were reacted with RB-NB. Each parallel exposed to the laser for 15 min at a density of 0.7 W/cm^2. Cells were harvested using 0.05% trypsin after 24 h incubation and washed twice with cold PBS, and then suspended in binding buffer. Then, 1×10^5 cells in 100 μL binding buffer were added to a tube and incubated with 5 μL of Annexin-V-FITC and 5 μL of PI. Cells were gently mixed and incubated for 15 min at room temperature. 400 μL binding buffer was then added to each tube. The samples were analyzed by flow cytometry (BD Biosciences). Experiments were repeated three times.

2.9. In vivo imaging and PDT

The mice experiments were performed in accordance with the animal regulations and management protocols. The tumors were developed by the subcutaneous injection of MCF-7 cells into nude mice. After the tumor volume grew to about 50 mm^3, the mice were randomly separated into different groups for study. After the post-injection of nanoplatforms, the mice were imaged with a modified IVIS system, which was equipped with a 980 nm light source. For PDT treatment, the mice were randomly divided into six groups (n = 5) (i) Saline, (ii) 980 nm light, (iii) UCNPs-Tz/FA-PEG alone (iv) UCNPs-FA-PEG and RB-NB with 980 nm irradiation (v) UCNPs-Tz/FA-PEG and RB-NB with 980 nm irradiation (vi) “Always On” UCNPs with 980 nm irradiation. The mice were injected with the same doses of UCNPs (0.65 mg/mouse), except for the control groups, and for the group iv and v, the RB-NB (1.1 μg/mouse) was injected *in situ*. For the irradiated groups, the mice were irradiated with 980 nm laser (0.6 W/cm^2 for 15 min, 3 min irradiation and 3 min interval), respectively. The tumor sizes and body weights of the mice were monitored during the 14 days of treatment. The volume of tumor was measured as Volume = ($L \times W^2/2$), where L (length) and W(width) are two tumor dimensions, respectively. After the various treatment, the main organs and tumor tissues of the mice were collected on the 14th day for further study after H&E staining.

2.10. Statistical analysis

Statistical data were analyzed applying one-way ANOVA test; C Pns > 0,05; D, P > 0,05, P** = 0,0075, P* = 0,036; E, Pns > 0,05. The shown data are mean ± SEM of all independent measurements.

3. Results and discussion

3.1. Synthesis and characterization of UCNPs-Tz/FA-PEG

To demonstrate the proof of concept we performed a strategy of real-time imaging and switchable PDT that can employ click chemistry to couple the photosensitizers with pre-injected imaging nanoparticles. The synthesis and characterization of click handles, including Tz, NB, and their derivatives are provided in Figs. S1 and S2. In anticipation of a significant increase of the reaction rate in more aqueous media, the click kinetics of Tz with NB in different solvents were exploited (Fig.

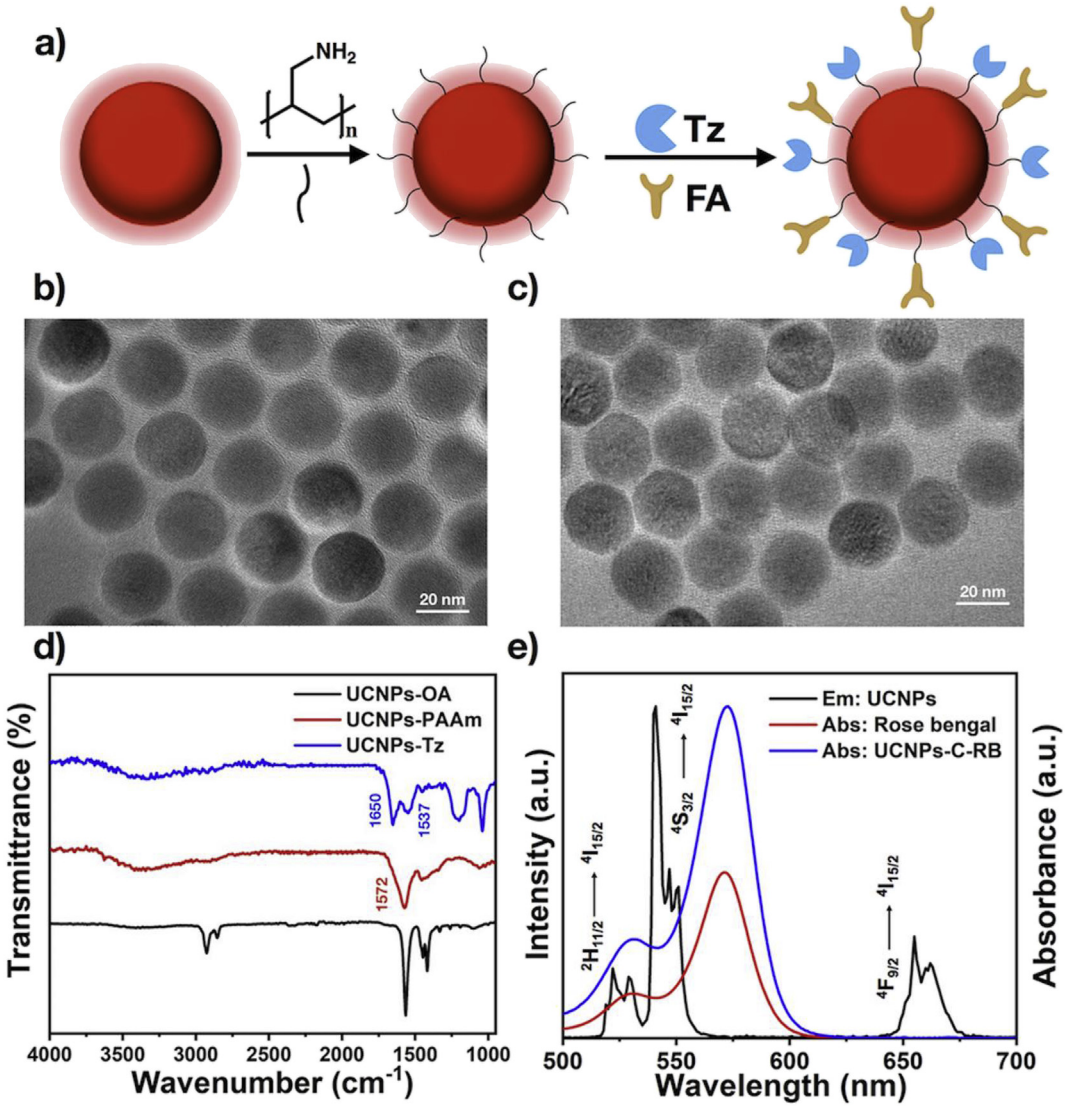

Fig. 1. Synthesis and characterization of the nanoplatform UCNPs-Tz/FA-PEG. a) Schematics of design and synthesis of UCNPs-Tz/FA-PEG. The morphology (TEM image) of b) UCNPs-OA, and c) UCNPs-Tz/FA-PEG. d) FTIR absorption spectra of UCNPs-OA, UCNPs-PAAm, and UCNPs-Tz. e) UCL spectra of UCNPs (in black); absorption of rose bengal (in red) and UCNPs-C-RB (in blue). (For interpretation of the references to color in this figure legend, the reader is referred to the Web version of this article.)

S3). The reaction rate was more than 20 $M^{-1} s^{-1}$ in PBS that is in solvent mixtures of higher water content, as expected, which is significant in bio-system.

The UCNPs-Tz/FA-PEG nanoplatform was prepared as illustrated in Fig. 1a. The $NaYF_4$: Yb, Er@$NaYF_4$ UCNPs were prepared according to reported protocol [35]. According to the thermogravimetry analysis (TGA) (20–600 °C, Ar) of nanoparticle $NaYF_4$: Yb, Er (Fig. S4), there is around 10% mass loss due to the organic ligands of the particles, and the synthesis yield is 64.1%. Subsequently, the as-synthesized oleic acid-capped UCNPs (UCNPs-OA) were functionalized with poly (allylamine) (PAAm) to obtain the hydrophilic amine-terminated UCNPs (NH_2-UCNPs). Afterwards, the click reaction handle Tz and tumor targeting moieties folic acid (FA) [36] were covalently conjugated with the NH_2-UCNPs. In order to increase the biocompatibility of the UCNPs-Tz/FA, the PEG succinimidyl carbonate (PEG-SC) was modified on its surface to form UCNPs-Tz/FA-PEG nanoplatform. As shown in Fig. 1b, the UCNPs-OA are spherical and monodispersed with the average size of ~26 nm. After the surface functionalization, no obvious aggregation was observed (Fig. 1c), the UCNPs-PAAm are positively charged and turned to neutral of the UCNPs-Tz/FA-PEG (Fig. S5). The successful preparation of the UCNPs-Tz/FA-PEG is confirmed from the FTIR spectra (Fig. 1d). Compared to the UCNPs-OA, the N–H stretching vibration band at 1572 cm^{-1} appears after PAAm coating. After conjugating with Tz molecule, the new bands at 1650 cm^{-1} (CO) and 1537 cm^{-1} (N-H) of secondary amide were observed.

Next, we turn to the conjugation of UCNPs-Tz/FA-PEG with photosensitizers *via* click reaction. Importantly, no significant change of the upconversion luminescence (UCL) spectrum and intensity was observed after the functionalization of UCNPs with Tz (Fig. S6). According to previous works, the RB covalently assembled upconversion nanoparticles (UCNPs-RB) is a very efficient nanoplatform (a type of "always on" nanoplatform) for singlet oxygen ($^1O_2$) generation upon 980 nm laser irradiation [37], which was supported by the well spectral overlap of UCL spectrum and the RB absorption, as shown in Fig. 1e.

3.2. Click reaction

Now we go to the click reaction dynamics between UCNPs-Tz and RB-NB in the solution. Since the red UC emission (~654 nm) was not quenched by the photosensitizers, we normalized the emission peak at

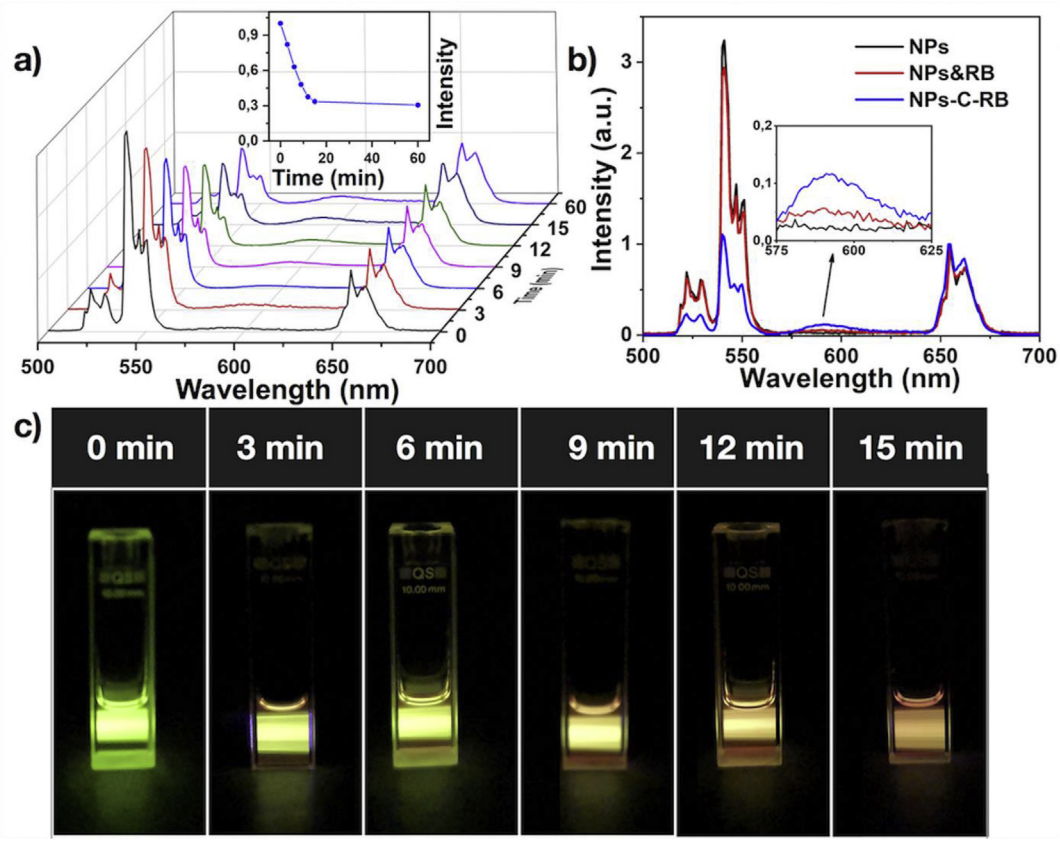

Fig. 2. a) The UCL spectra of the UCNPs reaction with RB-NB at a certain time, insert: relative intensity of integral area 535–560 nm. b) The UCL spectra of UCNPs-Tz/FA-PEG (black), UCNPs-FA-PEG mix with RB-NB (red) and UCNPs-Tz/FA-PEG click reaction with RB-NB (blue), normalized at 654 nm. c) Solution color of the UCNPs-Tz/FA-PEG reaction with RB-NB at a certain time. (For interpretation of the references to color in this figure legend, the reader is referred to the Web version of this article.)

654 nm to evaluate the click reaction rate, as shown in Fig. 2a. The UC emission at 535–560 nm is quenched by RB-NB and the relative integral turns from 1.0 (0 min) to 0.33 (15 min–60 min), verifying that the RB-NB was assembled to the UCNPs-Tz/FA-PEG *via* click reaction. It is worthwhile to note that the reaction finished within 15 min. This reaction speed is similar to that of click chemistry between the molecules, ensuring its application in biological systems. Given by these, the coupling yields were determined by the absorption spectra of the product after the cycloaddition. The maximum loading capacity is ~1.9% (RB weight/UCNP) corresponding to 200 RB/UCNP, which represents the Tz average loading capacity of each UCNP. The number of coupled RB can be further increased *via* increasing the amount of Tz. Due to the concentration quenching effect of the photosensitizers, we optimized the loading number of RB-NB molecules on the UCNPs, which was examined by using singlet oxygen indicator −1, 3-diphenylisobenzofuran (DPBF). The optimal loading capacity of RB-NB was confirmed around 1.7% (w/w, 190 RB/UCNPs), close to the maximum loading capacity, as shown in Fig. S7. It demonstrated that the nanophotosensitizers constructed covalently with click reaction are effective to produce $^1O_2$.

To further prove that this spectral change was attributed to the ET between UCNPs and RB molecules after the click reaction, the UCNPs without Tz moieties were taken as the control. The UC emission peak around 540 nm quenched significantly (green line) by the RB in the click covalently assembled NPs-C-RB (RB-NB/Tz-UCNPs), whereas no significant spectral change was observed without click reaction (RB-NB/UCNPs), as shown in Fig. 2b. Corresponding color changes from the non-Tz modified UCNPs to UCNPs-C-RB under irradiation of 980 nm laser were also observed, as shown in Fig. 2c, where UCNPs appear green (left), while UCNPs-C-RB becomes red (right). The ET efficiency is up to 72% when the click reaction occurs; on the contrary, only 12% is obtained. RB emission of NPs-C-RB was also observed at ~590 nm, confirming the effective ET from the UCNPs to RB. The result was also verified by DPBF consumption (Fig. S8), indicating that only the NPs-C-RB nanoplatforms can produce a significant amount of ROS for effective photoactivity.

3.3. Click reaction in vitro for imaging and therapy

Before *in vitro* and *in vivo* tests, it is an essence to assess the biocompatibility of the nanoplatforms. For that, the cell viability is determined over 86% in various concentration of the nanoplatforms (50, 100, 200 and 400 μg/mL), as shown in Fig. S9. Since the specific targeting of photosensitizers to the UCNPs is very important for the administration of cancer cells and tumors, the performance of the click chemistry targeting in cancer cells was thereby explored before the investigation of the PDT efficacy. To better investigate the click reaction *in vitro*, the other handle NB-FITC (green luminescence) was synthesized and employed. The human breast adenocarcinoma cells (MCF-7) were incubated overnight with UCNPs-Tz/FA-PEG which contain one handle Tz for click reaction and UCNPs-FA-PEG without click handle, respectively. After that, the red UCL from UCNPs was observed around the nucleus (blue fluorescence), as shown in Fig. 3, suggesting the cellular uptake of the UCNPs and the high feasibility of UCL imaging for the cancer cells. In order to achieve precise tracing of click reaction, the NB-FITC has to be the effective covalent linkage on targeted UCNPs-Tz/FA-PEG *via* the click reaction between Tz and NB. Indeed, the FITC was visualized clearly around the nucleus after 10 min and 20 min incubation, as well as exhibited similar imaging (green) with UCL (red). On the contrary, almost no FITC signal was observed in the control group

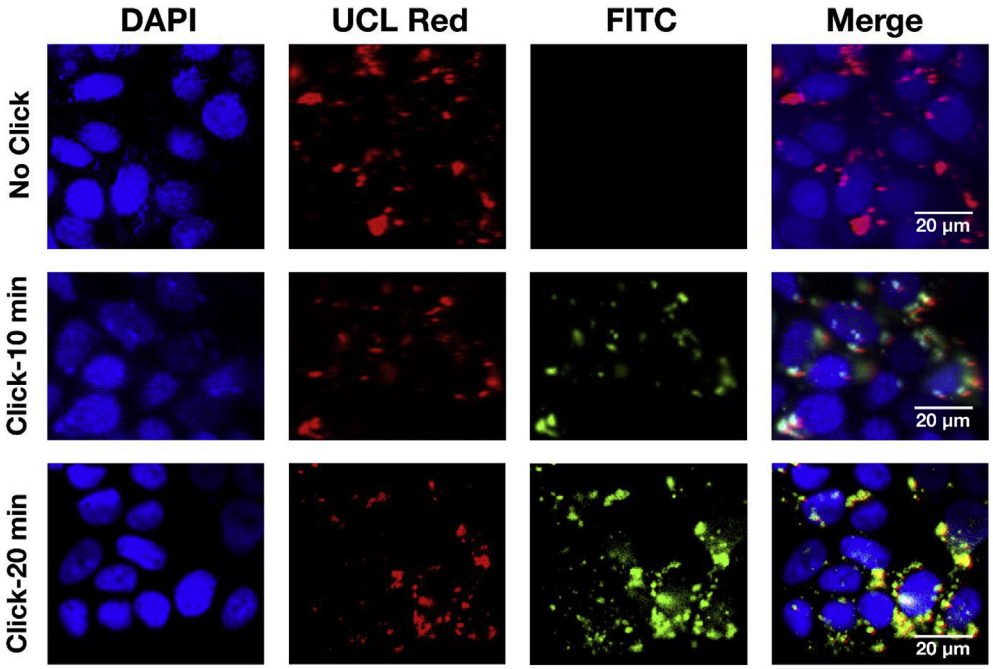

Fig. 3. MCF-7 cells treated with UCNPs-Tz/FA-PEG or UCNPs-FA-PEG for UCL imaging with 980 nm light excitation (red channel), and click reaction with FITC-NB (green channel), and stained with DAPI (blue channel). Top: control (no click), middle: click for 10 min and bottom: click for 20 min. Scale bars are marked. (For interpretation of the references to color in this figure legend, the reader is referred to the Web version of this article.)

where the NB-FITC was incubated with UCNPs-FA-PEG targeted cells. These results reassure that RB-NB was site-specifically and effectively localized on UCNPs-Tz/FA-PEG in living cell. Therefore, the high reaction rate of bioorthogonal click reaction in medium without toxic Cu (I) catalyst makes the click reaction suitable for *in situ* loading of PDT agent, *e.g.* RB to UCNPs-Tz labeled cells.

Encouraged by the above site-specific and effective click reaction and the UCL tumor cell-imaging performance, subsequently, the PDT effect of the two-step approach *in vitro* was studied by MTS assay. As shown in Fig. 4a, due to the powerful cancer cell destructing effect of the ROS, the group pretreated with UCNPs-Tz/FA-PEG and followed by RB-NB shows potent cellular inhibition upon 980 nm irradiation. The cell viability is 38% (50 μg/mL) and 22% (200 μg/mL), respectively, while the others are all over 80% without the click reaction. Significantly, destructing effect is at the similar level as the PDT employing "always on" nanoplatforms. Furthermore, we also studied the cell apoptosis resulted from click reaction-mediated PDT by flow cytometry. The Annexin-V-FITC/PI staining shown in Fig. 4b demonstrates that there is only 49.6% viable cells and 40.1% apoptotic cells in the group pretreated with UCNPs-Tz/FA-PEG and followed by RB-NB (click reaction), whereas 82.2% viable cells and only 13.5% apoptotic cells in the group without click reaction. The results indicate that UCNPs-Tz/FA-PEG has great potential for application as a PDT candidate and targeted imaging agent.

3.4. *In vivo* imaging and selective therapy

The blood tests were executed and the results are shown in Fig. S10 where no significant difference of RBC, WBC, and platelets before injection and 48 h after injection was observed. Next, we studied the UCL imaging performance *in vivo* to monitor tumor size/distribution for imaging-guided PDT because of its high-resolution visualization and deep tissue penetration. After intravenous (i.v.) injection of the nanoplatforms, the UCL images of tumor region were recorded at various times after injection, *i.e.* 30 min, 1 h, 2 h and 24 h. Strong UCL in the tumor sites was observed as shown in Fig. 5 when the mice were exposed to 980 nm laser light. It reveals that the nanoparticles were accumulated well in the tumor tissues owing to the FA targeting and EPR effect (Enhanced permeability and retention effect), which guarantees the UCL tracking and imaging-guided PDT.

Encouraged by the UCL imaging results, we then evaluated the PDT effect *in vivo via* click reaction with the photosensitizer. Here, we separated the tumor-bearing mice for 6 groups, as, "Saline", "Saline + 980 nm", "NPs-Tz/FA-PEG", "NPs-FA-PEG + RB-NB + 980 nm", NPs-Tz/FA-PEG + RB-NB + 980 nm" and "Always On + 980 nm" groups. The saline, NPs-Tz/FA-PEG (click), NPs-FA-PEG (no click), and the NPs-RB-PEG (always on) were intravenously administered, respectively. After 12 h post-injection of RB-NB, the mice were irradiated for 15 min (interval in every 3 min irradiation) with 980 nm laser at 0.6 W/cm^2, respectively. The relative tumor volumes were recorded to evaluate the PDT efficacy of this two-step strategy during 14 days of treatment. As shown in Fig. 6a and b, compared to "Saline" group, the group of NPs-Tz/FA-PEG + 980 nm and "NPs-FA-PEG + RB-NB + 980 nm (no click)" had negligible inhibition effect on tumor growth, the relative tumor size grew to 9–10 times larger than that of before. While the treatment of "NPs-Tz/FA-PEG + RB-NB + 980 nm" showed dramatical antitumor efficacy which was 75.5%, the antitumor efficacy was even comparable to "Always On + 980 nm" group (79.8%). These results reveal that the coupled photosensitizer (NB-RB) on the surface of nanoplatform by click reaction is successful in switching PDT on and showing satisfactory antitumor efficacy upon NIR light irradiation. Furthermore, there were no significant body weight losses (Fig. 6c) or abnormal behaviors observed. As illustrated by hematoxylin and eosin (H&E) examination, no significant damage to major organs was found in the treatment groups (Fig. 6d). On the contrary, significant damage was observed in both "NPs-Tz/FA-PEG + RB-NB + 980 nm" and "Always On + 980 nm" groups after the PDT treatment (Fig. 6e). These histological results further confirm the PDT effect of the nanophotosensitizers under NIR irradiation.

4. Conclusion

In summary, we have presented and validated an approach in realizing deep and long-time imaging and switchable PDT *via* a bioorthogonal chemical reaction. The nanoplatform without photosensitizers affords unique property of UCL for the tracking and imaging of deep-seated tumors and the photosensitizers demonstrate efficient targeting to the tumors for the therapy. This approach is demonstrated to be efficient and less harmful for healthy cells. Imaging with UCL nanoparticles and following up PDT is realized for the first time *via* click

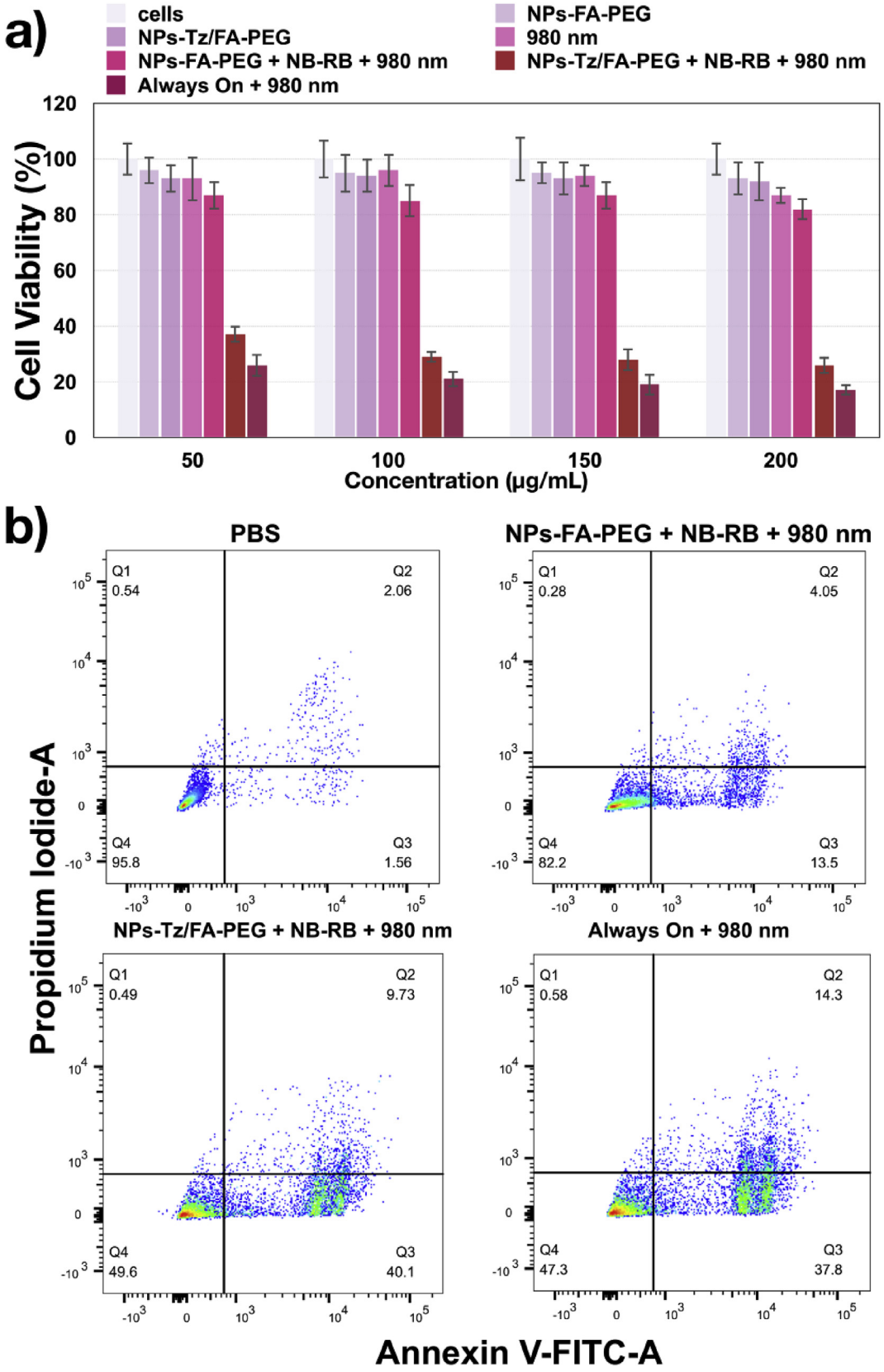

Fig. 4. a) Relative viabilities of cells for different treatments after being incubated with saline; NPs-Tz/FA-PEG; NPs-FA-PEG; conducted 980 nm laser; NPs-FA-PEG and NB-RB conducted with 980 nm; NPs-Tz/FA-PEG and NB-RB conducted with 980 nm; "Always on" UCNPs conducted with 980 nm. Excitation power density = 0.7 W/cm^2. b) Apoptosis of MCF-7 cells incubated with PBS or UCNPs-FA-PEG or UCNPs-Tz/FA-PEG or "Always On" under PDT treatment. The MCF-7 cells were stained by Annexin V-FITC, and analyzed by FACScan.

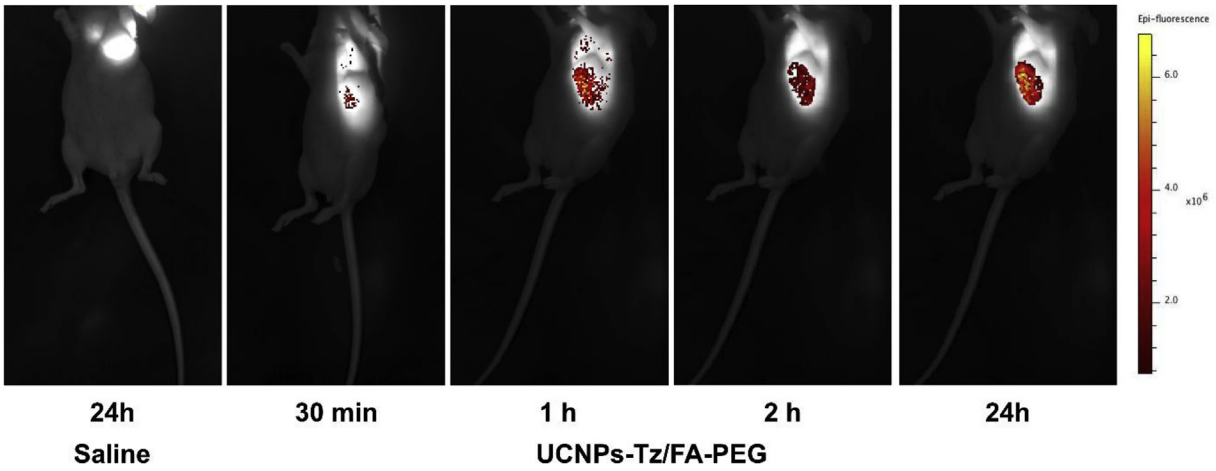

Fig. 5. *In vivo* UCL imaging of tumor-bearing mice with UCNPs-Tz/FA-PEG under irradiation of 980 nm laser at 30 min, 1 h, 2 h and 24 h after intravenous injection.

reaction. The *in vitro* and *in vivo* test results demonstrate the power of this strategy in precision medicine on cancer administration.

Conflicts of interest

The authors declare no conflict of interest.

Acknowledgements

This work was financially supported by Netherlands Organization for Scientific Research in the framework of the Fund New Chemical Innovation under grant nr.731.015.206, EU H2020-MSCA-ITN-ETN Action program, ISPIC, under grant nr. 675743, EU H2020-MSCA-RISE Action program, CANCER, under grant nr. 777682, EU H2020-MSCA-RISE-2014, PRISAR, under grant nr. 644373, joint research program between CAS of China and KNAW of the Netherlands, National Natural Science Foundation of China (11474278, 11674316, 21304084, 11374297, 61575194, 11504371 and 11604331), Project of Science and Technology Agency, Jilin Province (20170520112JH, 20170520113JH, 20170519002JH, and 20180101222JC).

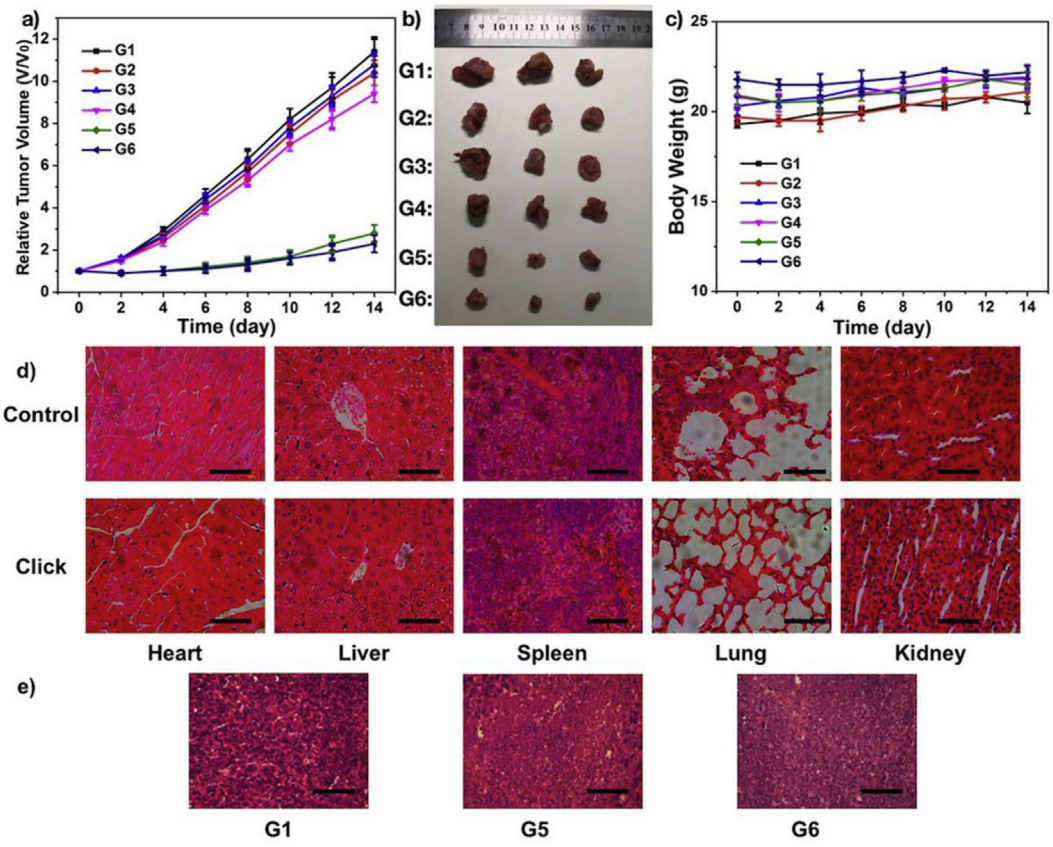

Fig. 6. a) Relative tumor volumes change during the treatment. b) Photographs to display the excised tumors after various treatment. c) Mice weight change during the treatment. G1: saline; G2: 980 nm only; G3: UCNPs-Tz/FA-PEG only; G4: UCNPs-FA-PEG + RN-NB + 980 nm; G5: UCNPs-Tz/FA-PEG + RN-NB + 980 nm; G6: "Always On" UCNPs +980 nm. d) The H&E staining of heart, liver, spleen, lung and kidney tissues in control and click groups. e) The H&E staining of tumors in G1, G5, and G6. The scar bars are 50 μm.

Appendix A. Supplementary data

Supplementary data to this article can be found online at https://doi.org/10.1016/j.biomaterials.2019.02.015.

References

[1] D.E.J.G.J. Dolmans, D. Fukumura, R.K. Jain, Photodynamic therapy for cancer, Nat. Rev. Canc. 3 (2003) 380–387.

[2] D. van Straten, V. Mashayekhi, H.S. de Bruijn, S. Oliveira, D.J. Robinson, Oncologic photodynamic therapy: basic principles, current clinical status and future directions, Cancers 9 (2) (2017) 19.

[3] T.J. Dougherty, G.B. Grindey, R. Fiel, K.R. Weishaupt, D.G. Boyle, Photoradiation therapy. II. Cure of animal tumors with hematoporphyrin and light, J. Natl. Cancer Inst. 55 (1) (1975) 115–121.

[4] J.P. Celli, B.Q. Spring, I. Rizvi, C.L. Evans, K.S. Samkoe, S. Verma, B.W. Pogue, T. Hasan, Imaging and photodynamic therapy: mechanisms, monitoring, and optimization, Chem. Rev. 110 (5) (2010) 2795–2838.

[5] S.S. Lucky, K.C. Soo, Y. Zhang, Nanoparticles in photodynamic therapy, Chem. Rev. 115 (4) (2015) 1990–2042.

[6] B.Y.S. Kim, J.T. Rutka, W.C.W. Chan, Nanomedicine, N. Engl. J. Med. 363 (25) (2010) 2434–2443.

[7] T. Sabri, P.D. Pawelek, J.A. Capobianco, Dual activity of rose bengal functionalized to albumin-coated lanthanide-doped upconverting nanoparticles: targeting and photodynamic therapy, ACS Appl. Mater. Interfaces 10 (32) (2018) 26947–26953.

[8] T.J. Dougherty, C.J. Gomer, B.W. Henderson, G. Jori, D. Kessel, M. Korbelik, J. Moan, Q. Peng, Photodynamic therapy, J. Natl. Cancer Inst. 90 (12) (1998) 889–905.

[9] Y.N. Konan, R. Gurny, E. Allémann, State of the art in the delivery of photosensitizers for photodynamic therapy, J. Photochem. Photobiol., A 66 (2) (2002) 89–106.

[10] D. Bechet, P. Couleaud, C. Frochot, M.-L. Viriot, F. Guillemin, M. Barberi-Heyob, Nanoparticles as vehicles for delivery of photodynamic therapy agents, Trends Biotechnol. 26 (11) (2008) 612–621.

[11] W. Fan, P. Huang, X. Chen, Overcoming the Achilles' heel of photodynamic therapy, Chem. Soc. Rev. 45 (23) (2016) 6488–6519.

[12] M.K.G. Jayakumar, N.M. Idris, Y. Zhang, Remote activation of biomolecules in deep tissues using near-infrared-to-UV upconversion nanotransducers, Proc. Natl. Acad. Sci. U.S.A. 109 (22) (2012) 8483.

[13] E. Hemmer, A. Benayas, F. Légaré, F. Vetrone, Exploiting the biological windows: current perspectives on fluorescent bioprobes emitting above 1000 nm, Nanoscale Horizons 1 (3) (2016) 168–184.

[14] N.M. Idris, M.K.G. Jayakumar, A. Bansal, Y. Zhang, Upconversion nanoparticles as versatile light nanotransducers for photoactivation applications, Chem. Soc. Rev. 44 (6) (2015) 1449–1478.

[15] N.M. Idris, M.K. Gnanasammandhan, J. Zhang, P.C. Ho, R. Mahendran, Y. Zhang, In vivo photodynamic therapy using upconversion nanoparticles as remote-controlled nanotransducers, Nat. Med. 18 (2012) 1580.

[16] Y.I. Park, H.M. Kim, J.H. Kim, K.C. Moon, B. Yoo, K.T. Lee, N. Lee, Y. Choi, W. Park, D. Ling, K. Na, W.K. Moon, S.H. Choi, H.S. Park, S.-Y. Yoon, Y.D. Suh, S.H. Lee, T. Hyeon, Theranostic probe based on lanthanide-doped nanoparticles for simultaneous in vivo dual-modal imaging and photodynamic therapy, Adv. Mater. 24 (42) (2012) 5755–5761.

[17] Q. Yuan, Y. Wu, J. Wang, D. Lu, Z. Zhao, T. Liu, X. Zhang, W. Tan, Targeted bioimaging and photodynamic therapy nanoplatform using an aptamer-guided G-quadruplex DNA carrier and near-infrared light, Angew. Chem. Int. Ed. 52 (52) (2013) 13965–13969.

[18] W. Fan, B. Shen, W. Bu, F. Chen, Q. He, K. Zhao, S. Zhang, L. Zhou, W. Peng, Q. Xiao, D. Ni, J. Liu, J. Shi, A smart upconversion-based mesoporous silica nanotheranostic system for synergetic chemo-/radio-/photodynamic therapy and simultaneous MR/UCL imaging, Biomaterials 35 (32) (2014) 8992–9002.

[19] L. Bu, B. Shen, Z. Cheng, Fluorescent imaging of cancerous tissues for targeted surgery, Adv. Drug Deliv. Rev. 76 (2014) 21–38.

[20] J. Akimoto, Photodynamic therapy for malignant brain tumors, Neurol. Med.-Chir. 56 (4) (2016) 151–157.

[21] J.S. Friedberg, R. Mick, J.P. Stevenson, T. Zhu, T.M. Busch, D. Shin, D. Smith, M. Culligan, A. Dimofte, E. Glatstein, S.M. Hahn, Phase II trial of pleural photodynamic therapy and surgery for patients with non–small-cell lung cancer with pleural spread, J. Clin. Oncol. 22 (11) (2004) 2192–2201.

[22] J. Gao, J. Li, W.-C. Geng, F.-Y. Chen, X. Duan, Z. Zheng, D. Ding, D.-S. Guo, Biomarker displacement activation: a general host–guest strategy for targeted phototheranostics in vivo, J. Am. Chem. Soc. 140 (14) (2018) 4945–4953.

[23] K. Zhou, Y. Wang, X. Huang, K. Luby-Phelps, B.D. Sumer, J. Gao, Tunable, ultrasensitive pH-responsive nanoparticles targeting specific endocytic organelles in living cells, Angew. Chem. Int. Ed. 50 (27) (2011) 6109–6114.

[24] J. Zuo, L. Tu, Q. Li, Y. Feng, I. Que, Y. Zhang, X. Liu, B. Xue, L.J. Cruz, Y. Chang, H. Zhang, X. Kong, Near infrared light sensitive ultraviolet–blue nanophotoswitch for imaging-guided "Off–On" therapy, ACS Nano 12 (4) (2018) 3217–3225.

[25] F. Li, Y. Du, J. Liu, H. Sun, J. Wang, R. Li, D. Kim, T. Hyeon, D. Ling, Responsive assembly of upconversion nanoparticles for pH-activated and near-infrared-triggered photodynamic therapy of deep tumors, Adv. Mater. 30 (35) (2018) 1802808.

[26] H.C. Kolb, M.G. Finn, K.B. Sharpless, Click chemistry: diverse chemical function from a few good reactions, Angew. Chem. Int. Ed. 40 (11) (2001) 2004–2021.

[27] J.-P. Meyer, P. Adumeau, J.S. Lewis, B.M. Zeglis, Click chemistry and radiochemistry: the first 10 years, Bioconjug. Chem. 27 (12) (2016) 2791–2807.

[28] R. Hoogenboom, Click chemistry for biotechnology and materials science, Angew. Chem. Int. Ed. 49 (20) (2010) 3410–3411 Edited by Joerg Lahann.

[29] A.-C. Knall, C. Slugovc, Inverse electron demand Diels–Alder (iEDDA)-initiated conjugation: a (high) potential click chemistry scheme, Chem. Soc. Rev. 42 (12) (2013) 5131–5142.

[30] E.M. Sletten, C.R. Bertozzi, A bioorthogonal quadricyclane ligation, J. Am. Chem. Soc. 133 (44) (2011) 17570–17573.

[31] E.M. Sletten, C.R. Bertozzi, From mechanism to mouse: a tale of two bioorthogonal reactions, Acc. Chem. Res. 44 (9) (2011) 666–676.

[32] N.A. B, S. Carsten, Selective fluorescence labeling of lipids in living cells, Angew. Chem. Int. Ed. 48 (8) (2009) 1498–1500.

[33] T. Plass, S. Milles, C. Koehler, C. Schultz, E.A. Lemke, Genetically encoded copper-free click chemistry, Angew. Chem. Int. Ed. 50 (17) (2011) 3878–3881.

[34] J. Yang, M.R. Karver, W. Li, S. Sahu, N.K. Devaraj, Metal-catalyzed one-pot synthesis of tetrazines directly from aliphatic nitriles and hydrazine, Angew. Chem. Int. Ed. 51 (21) (2012) 5222–5225.

[35] N.J.J. Johnson, A. Korinek, C. Dong, F.C.J.M. van Veggel, Self-focusing by ostwald ripening: a strategy for layer-by-layer epitaxial growth on upconverting nanocrystals, J. Am. Chem. Soc. 134 (27) (2012) 11068–11071.

[36] R.I. Pinhassi, Y.G. Assaraf, S. Farber, M. Stark, D. Ickowicz, S. Drori, A.J. Domb, Y.D. Livney, Arabinogalactan – Folic Acid – Drug conjugate for targeted delivery and target-activated release of anticancer drugs to folate receptor-overexpressing cells, Biomacromolecules 11 (1) (2010) 294–303.

[37] K. Liu, X. Liu, Q. Zeng, Y. Zhang, L. Tu, T. Liu, X. Kong, Y. Wang, F. Cao, S.A.G. Lambrechts, M.C.G. Aalders, H. Zhang, Covalently assembled NIR nanoplatform for simultaneous fluorescence imaging and photodynamic therapy of cancer cells, ACS Nano 6 (5) (2012) 4054–4062.